

Interplay of single-particle and collective modes in the $^{12}\text{C}(\text{p},2\text{p})$ reaction near 100 MeV

A. Deltuva^a, E. Cravo^{b,c}, R. Crespo^{d,e}, D. Jurčiukonis^a

^a*Institute of Theoretical Physics and Astronomy, Vilnius University, Saulėtekio al. 3, LT-10257 Vilnius, Lithuania*

^b*Departamento de Física, Faculdade de Ciências, Universidade de Lisboa, Campo Grande, 1749-016 Lisboa, Portugal*

^c*Centro de Física Teórica e Computacional, Faculdade de Ciências, Universidade de Lisboa, Campo Grande, 1749-016 Lisboa, Portugal*

^d*Departamento de Física, Instituto Superior Técnico, Universidade de Lisboa, Av. Rovisco Pais 1, 1049-001, Lisboa, Portugal*

^e*Centro de Ciências e Tecnologias Nucleares, Universidade de Lisboa, Estrada Nacional 10, 2695-066 Bobadela, Portugal*

Abstract

The $^{12}\text{C}(\text{p},2\text{p})^{11}\text{B}$ reaction at $E_p=98.7$ MeV proton beam energy is analyzed using a rigorous three-particle scattering formalism extended to include the internal excitation of the nuclear core or residual nucleus. The excitation proceeds via the core interaction with any of the external nucleons. We assume the ^{11}B ground and low-lying excited states [$\frac{3}{2}^-$ (0.0 MeV), $\frac{5}{2}^-$ (4.45 MeV), $\frac{7}{2}^-$ (6.74 MeV)] and the excited states [$\frac{1}{2}^-$ (2.12 MeV), $\frac{3}{2}^-$ (5.02 MeV)] to be members of $K = \frac{3}{2}^-$ and $K = \frac{1}{2}^-$ rotational bands, respectively. The dynamical core excitation results in a significant cross section for the reaction leading to the $\frac{5}{2}^-$ (4.45 MeV) excited state of ^{11}B that cannot be populated through the single-particle excitation mechanism. The detailed agreement between the theoretical calculations and data depends on the used optical model parametrizations and the kinematical configuration of the detected nucleons.

Key words:

Few-body reactions, proton removal, core excitation.

1. Introduction

The one-nucleon removal reactions have been extensively used to study the single-particle configurations of the involved nucleus A and the population of the states of its $B = (A - 1)$ residue. At the same time, it is becoming widely accepted that single-particle, molecular/cluster and collective degrees of freedom of a nuclei coexist along the nuclear landscape. These rich aspects of the nuclear structure are standardly described by shell models, cluster and collective structure models, respectively [1–4]. Concurrently, *ab initio* models that solve the Schrödinger equation for the many-body system of protons and neutrons have been developed with Hamiltonians based on the fundamental theory of the strong interactions [5] or effective interactions [6].

Despite tremendous advances in reaction and structure, Nuclear Physics has been indulging in the artificial separation between these two branches, notwithstanding one aims to extract nuclear properties from reactions. Some progress have been made recently to fully describe bound and scattering states or to some extent incorporate a many-body description of the nucleus into reactions [7–12]. Within the

later approach, *ab initio* shell-model-like Variational Monte Carlo (VMC) wave functions (WFs) [6] were recently employed to model the single-nucleon removal from light nuclei [9–11] under the inert-core assumption where the knock-out/breakup operator does not change the internal structure of the core. As a result of this crucial assumption, the one-nucleon spectroscopic overlap defined as a projection of the parent nucleus A state onto an antisymmetrized core + valence nucleon ($B + N$) form [11,13] becomes a key structure input for the reaction formalism. For a given state of the residual nucleus, the one-nucleon spectroscopic overlap is a superposition of different nucleon angular momentum channels, ℓ_j , satisfying the appropriate triangular relations [13]. The strength of the overlap or the so called spectroscopic factor (SF) for a given transition is obtained from the integral of the one-nucleon overlap function in each angular momentum channel. The systematic study of p-shell nuclei via the single-nucleon removal channel reactions has shown that the VMC WFs may overpredict the experimental data by almost a factor of two for light systems [9]. This discrepancy raises a question on the reaction model, in particular, the validity of the underlying inert-core assump-

tion. Furthermore, this reaction model is unable to predict the cross sections for the residue B states absent in the initial nucleus A , i.e., those with (almost) vanishing overlap and SF.

The ^{12}C isotopes and isotones constitute a paradigmatic light nuclei sample in which it is possible to study the coexistence of different structure aspects and its signature in reactions. *Ab initio* VMC WFs for ^{12}C were recently employed in benchmark calculations of neutrinoless double beta decay [14] and for ^{11}B in studies of nuclear charge radii of boron isotopes [15]. Total cross sections, angular and energy distributions, and polarization observables for $^{12}\text{C}(p, 2p)$ were measured at GSI [16] and RCNP [17] in inverse and direct kinematics, respectively, around 400 MeV/A energy for the ground state $\frac{3}{2}^-$ and low-lying excited states $\frac{1}{2}^-$ (2.12 MeV) and $\frac{3}{2}^-$ (5.02 MeV) of ^{11}B . The VMC WFs were used to model the proton-removal reaction $(p, 2p)$ [10,11] using standard few-body reaction frameworks where the final residue remains inert during the scattering process. It was found that the VMC spectroscopic strength appears to be distributed among the low lying states differently than the deduced experimental values, and that the agreement between the data and predictions using these *ab initio* WFs diminishes prominently for transitions to excited states of ^{11}B [10,11].

Furthermore, the $^{12}\text{C}(p, 2p)$ reaction was also measured at a lower energy of 98.7 MeV in direct kinematics at the Indiana University Cyclotron Facility (IUCF), capable to separate the ground $\frac{3}{2}^-$ and low-lying excited $\frac{1}{2}^-$ (2.12 MeV), $\frac{5}{2}^-$ (4.45 MeV) and $\frac{3}{2}^-$ (5.02 MeV) negative-parity states of ^{11}B [18]. The outgoing protons were detected in a coplanar geometry, in two different geometries around the Quasi Free Scattering (QFS) or no-core-recoil condition. This experiment has shown a strong population of the $\frac{5}{2}^-$ (4.45 MeV) state that cannot be understood from the dominance of the single-particle knockout.

Meanwhile, single particle and collective aspects of nuclear structure have been incorporated in few-cluster nuclear reactions. The collective mode, simulated as a dynamical excitation of the nuclear core, was found to play an important and characteristic role in three-cluster breakup reactions [19–26].

In this manuscript we aim to reanalyze the IUCF data taking into account dynamical excitation of the ^{11}B core during the scattering process and get insight in the $(p, 2p)$ reaction mechanisms. In particular, whether the core excitation mechanism can be responsible for the transitions to ^{11}B states with vanishing SF in the initial ^{12}C .

2. Formalism

We use the Faddeev formalism [27] for three-particle scattering, but extended to include the internal excitation of the nuclear core, i.e., the residual nucleus $(A - 1)$, labeled B for the brevity. The excitation proceeds via the core in-

teraction with any of the external nucleons. We work with generalized three-body transition operators of Alt, Grassberger, and Sandhas (AGS) [28]. Below we shortly recall the basic equations, whereas a more detailed description can be found in earlier works [26].

We use the usual odd-man-out notation, where, for example, the channel $\alpha = 1$ implies the particle 1 being a spectator while particles 2 and 3 build a pair; Greek subscripts are used for this notation. Since the nuclear core B can be excited or deexcited when interacting with nucleons, we introduce additional Latin superscript labels for the internal state of the core, either ground (g) or excited (x). The two-particle potentials v_α^{ba} , the two-body transition operators

$$T_\alpha^{ba} = v_\alpha^{ba} + \sum_c v_\alpha^{bc} G_0^c T_\alpha^{ca}, \quad (1)$$

as well as the resulting three-body transition operators

$$U_{\beta\alpha}^{ba} = \bar{\delta}_{\beta\alpha} \delta_{ba} G_0^{a-1} + \sum_{\gamma,c} \bar{\delta}_{\beta\gamma} T_\gamma^{bc} G_0^c U_{\gamma\alpha}^{ca}. \quad (2)$$

couple those sets of states. The operators (1) and (2) include simultaneously both core excitation and single-particle-like excitations, making those contributions mutually consistent. Here $\bar{\delta}_{\beta\alpha} = 1 - \delta_{\beta\alpha}$, E is the available system energy in the c.m. frame, and $G_0^a = (E + i0 - \delta_{ax} \Delta m_B - H_0)^{-1}$ is the free resolvent that beside the internal-motion kinetic energy operator H_0 contains also the contribution of the excitation energy Δm_B . In this formalism the two-nucleon potential v_α^{ba} and the respective transition matrix T_α^{ba} have only diagonal components $b = a$. The breakup operator

$$U_{0\alpha}^{ba} = \delta_{ba} G_0^{a-1} + \sum_{\gamma,c} T_\gamma^{bc} G_0^c U_{\gamma\alpha}^{ca}, \quad (3)$$

corresponds to the case $\beta = 0$ in Eqs. (2) and, once the coupled system for $\beta = 1, 2, 3$ is solved, does not require a new solution of Eqs. (2) but is given by the quadrature (3) involving $U_{\gamma\alpha}^{ca}$ with $\gamma = 1, 2, 3$.

The physical amplitudes for the breakup process are obtained as the on-shell matrix elements of $U_{0\alpha}^{ba}$ taken between initial and final channel states. We label by $\alpha = 1$ the initial two-cluster state, where the proton with the relative momentum \mathbf{q}_1 impinges on the nucleus $(B + N)$, i.e., $|\Phi_1(\mathbf{q}_1)\rangle = (|\Phi_1^g\rangle + |\Phi_1^x\rangle)|\mathbf{q}_1\rangle$. The spectator part $|\mathbf{q}_1\rangle$ is a free wave while the pair part $|\Phi_1^g\rangle + |\Phi_1^x\rangle$ is a solution of the Schrödinger equation with a real $(B + N)$ potential that couples ground- and excited-state core components. In the core-valence bound-state partial-wave (0^+ in the case of ^{12}C) the same potential has to be used also for the transition operator in Eq. (1) where it generates the bound-state pole. This special potential (see Appendix A) is taken to have Woods-Saxon form with central and spin-orbit terms plus Coulomb, and its parameters are adjusted such that the resulting two-body wave-function components in the r -space $\Phi_1^a(r)$ reproduce (up to a factor) the corresponding VMC spectroscopic overlaps $R^a(r)$ defined in Ref. [13], i.e.,

$\Phi_1^a(r) = \mathcal{N}^{-1/2} R^a(r)$. The procedure is similar to the one proposed in Ref. [13] but with an important extension including the g - x channel coupling. The normalization factor \mathcal{N} is introduced to ensure that $|\Phi_1^g\rangle + |\Phi_1^x\rangle$ is normalized to unity as required by the AGS equations (2). Since the norm of the spectroscopic overlap $R^a(r)$ is by definition the respective spectroscopic factor $SF(a)$, we have $\mathcal{N} = SF(g) + SF(x)$. Using the same \mathcal{N} for both g and x components ensures that their relative weight is preserved as in VMC overlaps. Thus, the spatial and momentum distributions of the initial channel wave function $|\Phi_1^g\rangle + |\Phi_1^x\rangle$ up to a normalization factor closely resemble those of the VMC overlaps.

We assume that in the final three-cluster channel $|\Phi_0^b(\mathbf{p}'_\eta, \mathbf{q}'_\eta)\rangle$ one can distinguish between the ground ($b = g$) and excited ($b = x$) states of the core. Instead of single-particle momenta \mathbf{k}_η we use Jacobi momenta, where \mathbf{p}'_η (\mathbf{q}'_η) labels the Jacobi momentum within the pair (spectator relative to the pair). The breakup channel states can be expressed in any of the three Jacobi sets η . Therefore, the amplitude for the three-cluster breakup reaction with the core nucleus in the final state b has to be calculated as

$$\mathcal{T}_1^b(\mathbf{p}'_\eta, \mathbf{q}'_\eta; \mathbf{q}_1) = \sum_a \langle \Phi_0^b(\mathbf{p}'_\eta, \mathbf{q}'_\eta) | U_{01}^{ba} | \Phi_1^a(\mathbf{q}_1) \rangle. \quad (4)$$

If the two nucleons are identical, the amplitude has to be properly antisymmetrized as discussed in Ref. [29].

We consider a kinematically complete three-particle breakup experiment where two particles, say, α and β , are detected at solid angles Ω_α and Ω_β , respectively. Measuring energy of one particle, E_α , in principle determines the final-state kinematics completely, since the remaining variables are constrained by the energy and momentum conservation (in the kinematical region of interest in the present work the relation between kinematic variables is unique, though in general it may have two solutions). The corresponding fivefold differential cross section is

$$\frac{d^5\sigma}{dE_\alpha d\Omega_\alpha d\Omega_\beta} = (2\pi)^4 \frac{M_1}{q_1} |\mathcal{T}_1^b(\mathbf{p}'_\eta, \mathbf{q}'_\eta; \mathbf{q}_1)|^2 \text{fps} \quad (5)$$

with $M_1 = m_1(m_2 + m_3)/(m_1 + m_2 + m_3)$, m_α being the mass of the particle α , and the phase-space factor

$$\text{fps} = \frac{m_\alpha m_\beta m_\gamma k_\alpha k_\beta^3}{|m_\gamma k_\beta^2 - m_\beta \mathbf{k}_\beta \cdot (\mathbf{Q} - \mathbf{k}_\alpha - \mathbf{k}_\beta)|}, \quad (6)$$

\mathbf{Q} being the total three-particle momentum.

We solve the scattering equations (2) and calculate the breakup amplitudes (3) in the momentum-space framework following Ref. [26], with a slight difference related to the inclusion of the Coulomb force. In the system of two protons and nuclear core the Coulomb force acts in all three pairs of particles, leading to unknown renormalization factor in the screening and renormalization procedure. We therefore include screened Coulomb potentials with respective strengths for all three pairs, but do not perform the renormalization of breakup amplitudes. Instead, we check that the cross sections to a good accuracy become indepen-

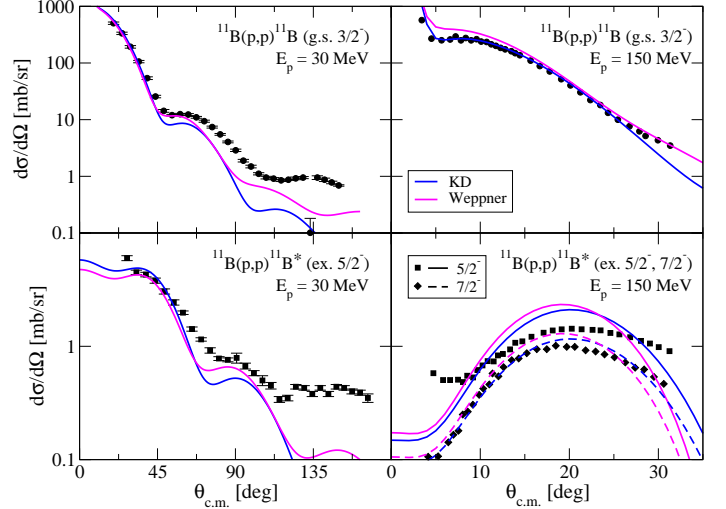


Fig. 1. Differential cross section for the elastic and inelastic scattering $^{11}\text{B}(p,p)^{11}\text{B}^*$ at $E_p = 30.3$ MeV and 150 MeV, leading to the member states of the $K = \frac{3}{2}^-$ rotational band. Predictions are based on two sets of optical potential parametrizations, KD and Weppner. The data is taken from Refs. [37] and [38].

dent of the screening radius, implying that the renormalization factor should be just a phase factor, and the screened Coulomb potential simulates well the actual Coulomb force acting in the breakup process. In the considered reaction the convergence is achieved with the Coulomb screening radius around 10 fm, but even neglecting the Coulomb force does not lead to significant changes, implying that the Coulomb force is quite irrelevant in the present case.

The nucleon-residual nucleus potentials with the core excitation are constructed in a standard way using the rotational model [33–35]. One starts with a single-channel optical potential whose radial dependence is usually parametrized in terms of the Woods-Saxon function. In the present study, and to investigate the uncertainties of the calculated cross sections associated with the choice of the optical potential (OP) parametrization, we take two global OPs. They were developed by Weppner *et al.* [30] and Koning and Delaroche (KD) [31], and fitted to $A \geq 12$ nuclei and $A \geq 24$ nuclei, respectively. Despite this restriction, the KD potential has been used for systematic studies along the nuclear landscape also for lighter nuclei [32], and reproduces the experimental nucleon-nucleus data with a reasonable quality as will be shown later. For any of these OPs we assume a permanent quadrupole deformation of the nucleus. This induces a coupling to the internal nuclear degrees of freedom $\hat{\xi}$ of the residual nucleus via the Woods-Saxon radius $R_j = R_{j0}[1 + \beta_2 Y_{20}(\hat{\xi})]$, β_2 being the quadrupole deformation parameter, and $\delta_2 = \beta_2 R_{j0}$ called the deformation length. In the case here considered it was assumed that the ground state of spin/parity $\frac{3}{2}^-$ and excited states $\frac{5}{2}^-$ (4.45 MeV) and $\frac{7}{2}^-$ (6.74 MeV) of the ^{11}B residual nucleus are members of the $K = \frac{3}{2}^-$ rotational band, while the excited states $\frac{1}{2}^-$ (2.12 MeV) and $\frac{3}{2}^-$ (5.02 MeV) are members of the $K = \frac{1}{2}^-$ rotational band

[36,37]. We use axially symmetric rotational model and do not include coupling between states belonging to different rotational bands. When looking at the experimental data for the proton + ^{11}B inelastic scattering [37,38] one notices that $K = \frac{3}{2}^-$ to $K = \frac{1}{2}^-$ cross sections are 3 to 5 times lower than those within the $K = \frac{3}{2}^-$ band, which justifies our approximation.

The experimental data for the proton + ^{11}B scattering, needed to fix the potential parameters, is available in the $K = \frac{3}{2}^-$ case only, and in different energy regime of $E_p=30.3$ MeV [36], suggesting $\beta_2 \approx 0.52$, or $\delta_2 \approx 1.5$ fm. We find this value consistent also with the experimental data at the higher energy of $E_p=150$ MeV [38]. Due to the lack of experimental information we use the same parameters also for the reactions coupling the states of the $K = \frac{1}{2}^-$ rotational band.

In summary, the used nucleon-residue potentials are based on the Weppner's and KD parametrizations with $\delta_2 \approx 1.5$ fm rotational quadrupole deformation length. An exception is the core-valence interaction in the 0^+ partial wave where real potentials (different for each band) are used to simulate VMC spectroscopic overlaps. As for the two-nucleon potential we verified that results are insensitive to its choice provided it is a realistic high-precision potential such as AV18 [40] or CD Bonn [41].

3. Results

Our main goal is to study the $^{12}\text{C}(p, 2p)$ reaction at the incident proton energy $E_p = 98.7$ MeV, measured in direct kinematics at the Indiana University Cyclotron Facility (IUCF) [18]. However, we begin by testing the adequacy of the chosen nucleon-nucleus dynamical excitation model with rotational quadrupole deformation. Due to the lack of experimental information around $E_p=100$ MeV we display in Fig. 1 the angular distributions of the differential cross section for elastic and inelastic scattering $^{11}\text{B}(p, p)^{11}\text{B}^*$ leading to the states of the $K = \frac{3}{2}^-$ rotational band, and compare them with the experimental data at $E_p=30.3$ MeV and $E_p=150$ MeV taken from Refs. [37] and [38], respectively. While at the lower energy the predictions using the Weppner's OP are somewhat closer to the data, at the higher energy the KD OP reproduces the data slightly better, while the Weppner OP tends to overestimate the cross sections. Nevertheless, the calculated proton- ^{11}B elastic and inelastic cross sections using both global OP parametrizations follow fairly well the trend of the data with the exception of the $\frac{5}{2}^-$ state in the forward-angle region where other multipolar transitions are expected to contribute [38]. Moreover, the data for the excitation of the $\frac{7}{2}^-$ state at 150 MeV are well reproduced.

Next, we solve the three-body Faddeev/AGS equations including the core excitation (here labelled as CX) and calculate the fivefold differential cross section for the $^{12}\text{C}(p, 2p)^{11}\text{B}$ reaction. In order to estimate the CX effect

we performed also the corresponding calculations without the core excitation, i.e., using the standard single-particle (SP) dynamic model [10].

The two particles detected in the Indiana experimental setup [18] are the two protons, to be labeled p and N in the following, though one has to keep in mind that they are indistinguishable and the scattering amplitudes are correspondingly antisymmetrized. The emitted protons are measured in a coplanar geometry, with the azimuthal angle between them being 180° . The plane geometry reduces the number of independent kinematical variables to three, chosen as the energy of one proton and polar angles of both protons, $\{E_p, \theta_p, \theta_N\}$. The outgoing protons were detected in two different kinematic geometries around the Quasi Free Scattering (QFS): A symmetric one, labeled KS in [18], is characterized by $E_p = 41.35 \pm 1.25$ MeV and $\theta_p = \theta_N$ taking five values from 30° to 65° . An asymmetric one, labeled KA in [18], is characterized by $E_p = 59.5 \pm 1.8$ MeV, $\theta_p = 25^\circ$, and θ_N taking five values from 30° to 90° .

The bound-state wave function in the three-body AGS calculations is normalized to unity, but multiplied by the normalization factor $\mathcal{N}^{1/2}$ its components reproduce the respective microscopic VMC overlaps. Therefore the spectroscopic VMC information is taken into account multiplying the AGS-CX cross section results by the norm factor $\mathcal{N} = \text{SF}(g) + \text{SF}(x)$ which is the sum of SFs for the states coupled in the AGS calculations. The AGS-SP calculations involve only a single state, in that case one has to multiply the cross section by the SF of the considered state, which is a standard way to include the spectroscopic information also into the distorted-wave calculations [10]. The VMC SFs for the $\frac{3}{2}^-$ (0.0 MeV), $\frac{1}{2}^-$ (2.12 MeV), $\frac{5}{2}^-$ (4.45 MeV), and $\frac{3}{2}^-$ (5.02 MeV) states of ^{11}B are 2.363, 0.819, 0.001, and 0.206, respectively [39].

The fivefold differential cross sections, scaled by the SF's in an appropriate way, are shown in Fig 2 as functions of the core momentum p_B . Results using both Weppner and KD OP parametrizations, with and without CX, for both KS (left) and KA (right) geometries are compared with the experimental data [18].

The general trend is that the CX effect increases the differential cross section in most parts of the considered kinematic region, CX predictions being higher than those of SP. In the case of the $\frac{5}{2}^-$ state the SP results are almost vanishing and are not shown. Another trend is that KD OP parametrization leads to higher differential cross section than Weppner OP, though in the two-body case the situation is reversed as shown in Fig. 1. This sensitivity is slightly enhanced in the CX case. All these features possibly indicate that the CX is a complicated phenomena resulting from interplay and partial cancellations of various terms in the dynamic equations, or, equivalently, in the multiple scattering series. In fact, if the multiple scattering series are replaced by the first-order terms only, the so-called single-scattering approximations (SSA), the resulting cross section is heavily enhanced. We illustrate this finding in

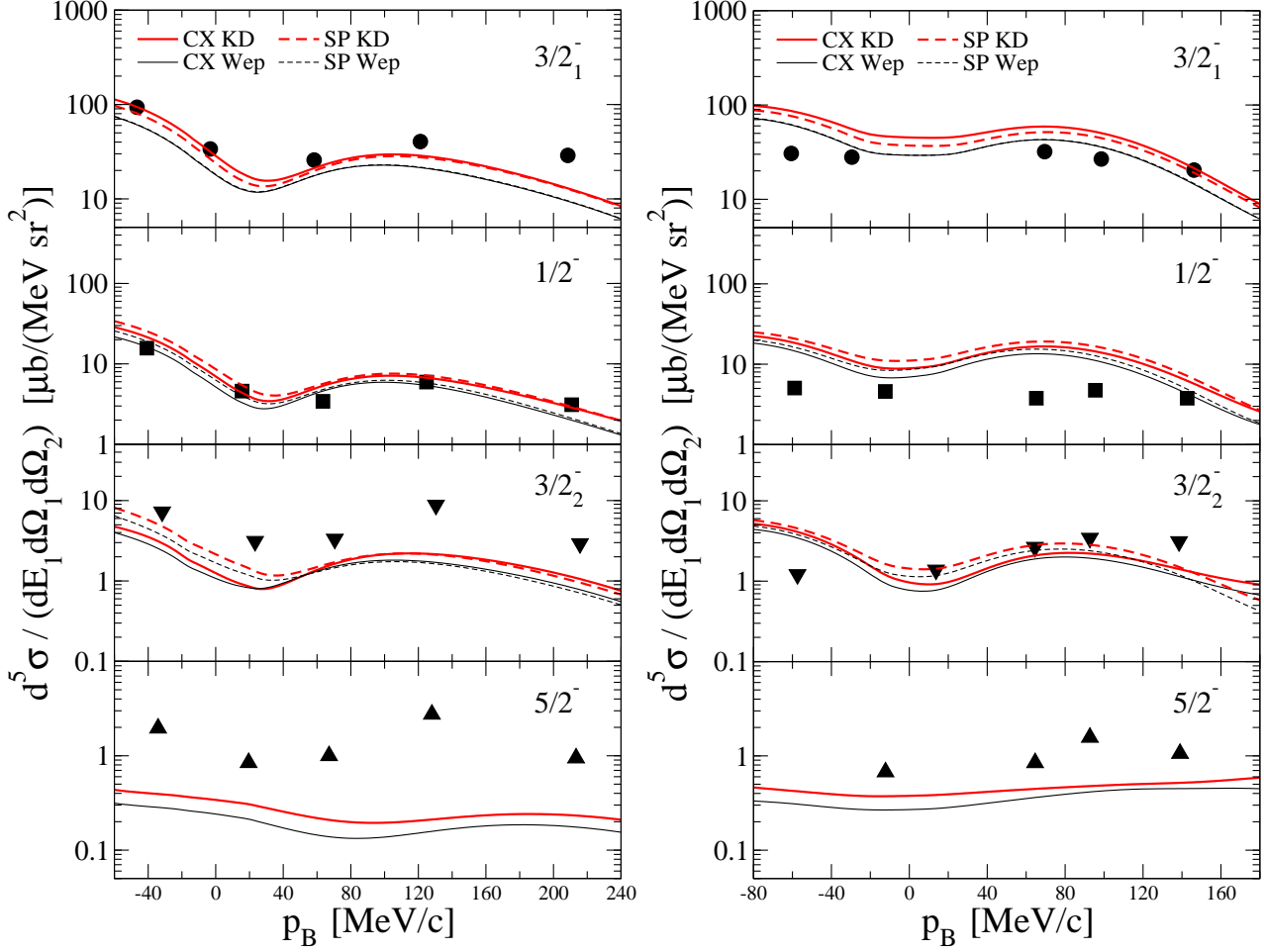


Fig. 2. Differential cross section for the $^{12}\text{C}(p, 2p)^{11}\text{B}$ reaction at $E_p = 98.7$ MeV as function of the residual nucleus momentum p_B in the symmetric (left) and asymmetric (right) kinematical settings of Ref. [18]. Predictions are based on the KD and Weppner (Wep) optical potential parametrizations, with the dynamical core excitation either included (CX, solid curves) or neglected (SP, dashed curves). The spectroscopic VMC information is taken into account as described in the text. The subscripts 1 and 2 distinguish the ground and excited $3/2^-$ states, respectively. The data is taken from Ref. [18].

Fig. 3 by comparing full results and SSA for transitions to the ground and $\frac{5}{2}^-$ state in the asymmetric kinematics. Despite that SSA cross sections are much higher, the CX effect for g.s. is qualitatively similar in both full and SSA cases. For curiosity we show also the SSA(pN) including only the proton-valence term. It excludes the proton-core interaction and thereby also the dynamic CX, leading to a vanishing CX effect. In the case of the $\frac{5}{2}^-$ state the SSA(pN) cross section is very small as a consequence of very small SF. Thus, it is indeed the dynamic CX that is responsible for an appreciable cross section for the final $\frac{5}{2}^-$ state.

With respect to reproducing the experimental data [18] the situation is quite contradictory. The differential cross section for the ^{11}B in its ground state $\frac{3}{2}^-$ is well described by the CX KD calculation in the KS kinematics and by SP and CX Weppner calculation in the KA kinematics. For the other member of the $K = \frac{3}{2}^-$ rotational band, the $\frac{5}{2}^-$ state, the differential cross section is significantly underestimated in the KS kinematics but only slightly underestimated in the KA kinematics by the CX KD calculation. For

the $K = \frac{1}{2}^-$ rotational band the transition to the excited state $\frac{1}{2}^-$ is quite well reproduced by all calculations in the KS kinematics but overpredicted in the KA kinematics. On the contrary, the transition to the excited state $\frac{3}{2}^-$ (5.02 MeV) is underestimated in the KS kinematics but, except for one point, described well by the KD calculations (both with and without CX) in the KA kinematics.

Thus, while in average the CX KD calculations appear to be more successful than the others, no single calculation provides a reasonable reproduction of all the experimental data [18]. The quality of the description depends on the kinematics, in the KS being better for the $\frac{3}{2}^-$ (0.0 MeV) and $\frac{1}{2}^-$ (2.12 MeV) states, while in KA being better for the $\frac{5}{2}^-$ (4.45 MeV) and $\frac{3}{2}^-$ (5.02 MeV) states. The reason remains unexplained.

Additionally, our models including dynamical core excitation predict differential cross section for the transition to the excited state $\frac{7}{2}^-$ to be smaller than the one for the $\frac{5}{2}^-$ but still of the same order of magnitude. We do not show it

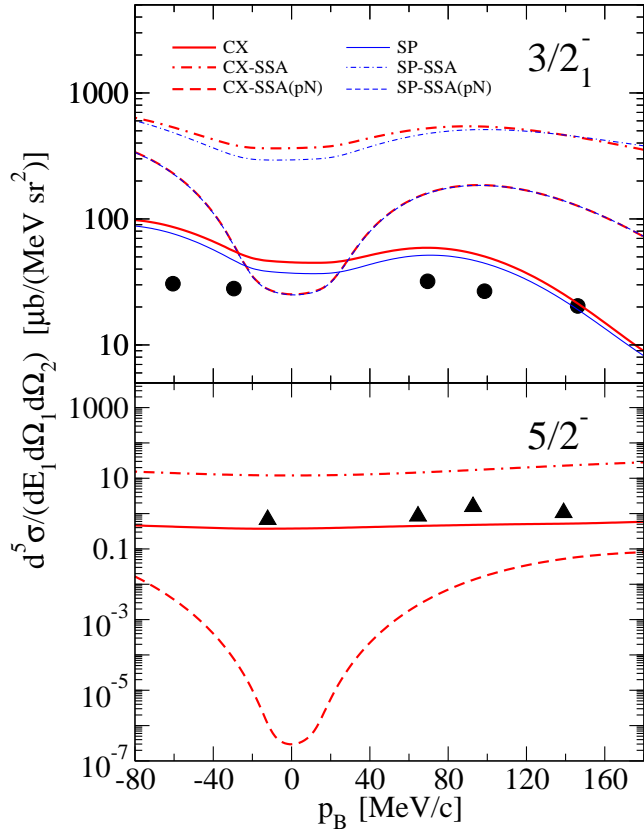


Fig. 3. Differential cross section for the $^{12}\text{C}(p,2p)^{11}\text{B}$ reaction at $E_p = 98.7$ MeV as function of the residual nucleus momentum p_B in the asymmetric kinematical setting of Ref. [18]. Predictions are based on the KD optical potential parametrization with the dynamical core excitation (CX, thick curves). For the ^{11}B ground state results neglecting CX are also shown (SP, thin curves). In both cases full results are given by solid curves while SSA results with proton-core and proton-valence (only proton-valence) terms are given by dashed-dotted (dashed) curves. The spectroscopic VMC information is taken into account as described in the text. The data is taken from Ref. [18].

here since the experimental data is not available for a pure state, only as a mixture with the $\frac{1}{2}^+$ state. In the same way as $\frac{5}{2}^-$, the transition to $\frac{7}{2}^-$ cannot be described by the SP model due to the associated negligible SF.

4. Summary and conclusions

We have reinterpreted the experimental data for the $^{12}\text{C}(p,2p)^{11}\text{B}$ reaction at $E_p = 98.7$ MeV, in which the emitted protons are measured in a coplanar geometry, with the azimuthal angle between them being 180° . Two kinematical settings have been considered.

We used an extended three-particle reaction formalism that includes the internal excitation of the nuclear core. The excitation proceeds via the core interaction with any of the external nucleons. We assume the ^{11}B ground and low-lying excited states [$\frac{3}{2}^-$, $\frac{5}{2}^-$ (4.45 MeV), $\frac{7}{2}^-$ (6.74 MeV)] and the excited states [$\frac{1}{2}^-$ (2.12 MeV), $\frac{3}{2}^-$ (5.02 MeV)] to be the members of the $K = \frac{3}{2}^-$ and $K = \frac{1}{2}^-$ rotational

Table A.1

Binding potential parameters for $K = \frac{3}{2}^-$ and $\frac{1}{2}^-$ rotational bands with quadrupole deformation length $\delta_2 = 1.5$ fm. The radii R_i and diffuseness a_i are in units of fm, central strength V_c is in units of MeV and spin-orbit strength V_{ls} is in units of MeV fm². The resulting weights of the ground- and excited state wave-function components are listed as well.

K	R_c	a_c	V_c	R_{ls}	a_{ls}	V_{ls}	V_{ss}/V_c	P_g	P_x
$\frac{3}{2}^-$	3.011	0.692	63.068	3.169	0.253	7.555	0.0	0.997	0.003
$\frac{1}{2}^-$	2.636	0.784	76.274	2.005	0.608	8.622	0.248	0.795	0.205

bands, respectively.

A detailed agreement between the theoretical calculations and data is somehow contradictory and depends on the used optical potential parametrization and the final-state kinematical situation. This possibly indicates that the core excitation is a complicated phenomena resulting from interplay and partial cancellations of various terms in the dynamic equations but also calls for a new data. Most importantly, the dynamical excitation of the core included in the reaction model predicts insufficient but nevertheless quite significant cross sections for transitions to the $\frac{5}{2}^-$ and $\frac{7}{2}^-$ excited states that cannot be populated via the single-particle excitation mechanism.

Thus, we have shown the ability to predict at least qualitatively the cross sections for states with residual nucleus components that are negligible in the initial nucleus. This will surely contribute also to analysis of upcoming data from $^{12}\text{C}(p,2p)^{11}\text{B}$ measurements detecting $\frac{5}{2}^-$ (4.45 MeV) and $\frac{7}{2}^-$ (6.74 MeV) states of ^{11}B , currently under study at GSI and other laboratories.

We thank R. B. Wiringa for providing the overlap functions. A.D. and D.J. are supported by Lietuvos Mokslo Taryba (Research Council of Lithuania) under Contract No. S-MIP-22-72. Part of the computations were performed using the infrastructure of the Lithuanian Particle Physics Consortium.

Appendix A. Nuclear binding potential

We start with an undeformed valence-core potential for the 0^+ state

$$v_1(r) = -V_c f(r, R_c, a_c) - \mathbf{s}_N \cdot \mathbf{s}_B V_{ss} f(r, R_c, a_c) + \mathbf{s}_N \cdot \mathbf{L} V_{ls} \frac{4}{r} \frac{d}{dr} f(r, R_{ls}, a_{ls}), \quad (\text{A.1})$$

where $f(r, R, a) = [1 + \exp((r - R)/a)]^{-1}$ is Woods-Saxon form factor, \mathbf{s}_N and \mathbf{s}_B are spins of the nucleon and nucleus, respectively, and \mathbf{L} is the orbital angular momentum. For the $K = \frac{1}{2}^-$ rotational band we found that appending the central term by a phenomenological spin-spin contribution suggested in Ref. [42] improves the fit significantly. To include excitation of the core, the central term is deformed in a standard way using $\delta_2 = 1.5$ fm. The parameters determined from the fit and the resulting weights P_a of the wave-function components are collected in Table A.1.

References

- [1] E. Caurier, G. Martinez-Pinedo, F. Nowacki, A. Poves, A.P. Zuker, *Rev. Mod. Phys.* 77, 427 (2005).
- [2] W. Von Oertzen, M. Freer, Y. Kanada-Enyo, *Phys. Rep.* 432, 43 (2006).
- [3] Y. Kanada-Enyo, T. Suhara, F. Kobayashi, *Eur. Phys. J.* 66, 01008 (2014).
- [4] A. Bohr and B.R. Mottelson, *Collective and Individual aspects of nuclear structure*, (1957).
- [5] R. Machleidt, D.R. Entem, *Phys. Rep.* 503, 1 (2011).
- [6] R. B. Wiringa, *et al.*, *Phys. Rev. C* 89, 024305 (2014).
- [7] S. Quaglioni and P. Navratil, *Phys. Rev. Lett.* 101, 092501 (2008).
- [8] F. Barranco *et al.*, *Phys. Rev. Lett.* 119, 082501 (2017).
- [9] G. F. Grinyer *et al.*, *Phys. Rev. C* 86, 024315 (2012).
- [10] A. Mecca, E. Cravo, A. Deltuva, R. Crespo, A.A. Cowley, A. Arriaga, R.B. Wiringa, T. Noro, *Phys. Lett. B* 798, 134989 (2019).
- [11] R. Crespo, A. Arriaga, R. Wiringa, E. Cravo, A. Deltuva, A.Mecca, *Phys. Lett. B* 803, 135355 (2020).
- [12] J. Rotureau, G. Potel, W. Li and F.M. Nunes, *J. Phys. G: Nucl. Part. Phys.* 47, 065103 (2020).
- [13] I. Brida, Steven C. Pieper and R. B. Wiringa, *Phys. Rev. C* 84, 024319 (2011).
- [14] X.B. Wang *et al.*, *Phys. Lett. B* 798,134974 (2019).
- [15] B. Maab, *et al.*, *Phys. Rev. Lett.* 122, 182501 (2019).
- [16] V. Panin, *et al.*, *Phys. Lett. B* 753, 204 (2016).
- [17] S. Kawase *et al.*, *Prog. Theor. Exp. Phys.* 2018, 021D01 (2018).
- [18] D.W. Devins, D.L. Friesel, W.P. Jones, A.C. Attard, I.D. Svalbe, v.C. Officer, R.S. Henderson, B.M. Spicer and G.G. Shute, *Aust. J. Phys.*, 32, 323 (1979).
- [19] A. M. Moro and R. Crespo, *Phys. Rev. C* 85, 054613 (2012).
- [20] A. Moro and J. A. Lay, *Phys. Rev. Lett.* 109, 232502 (2012).
- [21] N. C. Summers and F. M. Nunes, *Phys. Rev. C* 76, 014611 (2007).
- [22] R. de Diego, J. M. Arias, J. A. Lay, and A. M. Moro, *Phys. Rev. C* 89, 064609 (2014).
- [23] R. de Diego, R. Crespo, and A. M. Moro, *Phys. Rev. C* 95, 044611 (2017).
- [24] A. Deltuva, *Phys. Rev. C* 88, 011601(R) (2013).
- [25] A. Deltuva, D. Jurčiukonis, and E. Norvaišas, *Phys. Lett. B* 769, 202 (2017).
- [26] A. Deltuva, *Phys. Rev. C* 99, 024613 (2019).
- [27] L. D. Faddeev, *Zh. Eksp. Teor. Fiz.* 39, 1459 (1960), [*Sov. Phys. JETP* 12, 1014 (1961)].
- [28] E. O. Alt, P. Grassberger, and W. Sandhas, *Nucl. Phys.* B2, 167 (1967).
- [29] A. Deltuva, *Phys. Rev. C* 87, 034609 (2013).
- [30] S.P. Weppner, R.B. Penney, G.W. Diffendale and G. Vittorini, *Phys. Rev. C* 80, 034608 (2009).
- [31] A. J. Koning and J. P. Delaroche, *Nucl. Phys.* A713, 231 (2003).
- [32] E. Cravo, R. Crespo, and A. Deltuva, *Phys. Rev. C* 93, 054612 (2016).
- [33] A. Bohr and B. R. Motelson, *Nuclear Structure* (World Scientific, Singapore, 1998).
- [34] T. Tamura, *Rev. Mod. Phys.* 37, 679 (1965).
- [35] I. J. Thompson, *Computer Physics Reports* 7, 167 (1988).
- [36] Dinh-Liem Pham, *Le Journal de Physique Lett.* 37, L-67 (1976).
- [37] O. Karban, J. Lowe, P.D. Graves, V. Hnizdo, *Nucl. Phys.* A133 255 (1969).
- [38] V.M. Hannen et al, *Phys. Rev. C* 67, 054320 (2003).
- [39] R. B. Wiringa, <https://www.phy.anl.gov/theory/research/overlaps/>
- [40] R. B. Wiringa, V. G. J. Stoks, and R. Schiavilla, *Phys. Rev. C* 51, 38 (1995).
- [41] R. Machleidt, *Phys. Rev. C* 63, 024001 (2001).
- [42] K. Amos, L. Canton, G. Pisent, J. Svenne, D. van der Knijff, *Nucl. Phys.* A 728 (2003) 65.